DESIGN AND FIRST MEASUREMENTS OF AN ALTERNATIVE CALORIMETRY CHAMBER FOR THE HZB QUADRUPOLE RESONATOR

S. Keckert*, R. Kleindienst, J. Knobloch, O. Kugeler
Helmholtz-Zentrum Berlin, Germany

Abstract

The systematic research on superconducting thin films requires dedicated testing equipment. The Quadrupole Resonator (QPR) is a specialized tool to characterize the superconducting RF properties of circular planar samples. A calorimetric measurement of the RF surface losses allows the surface resistance to be measured with sub nano-ohm resolution. This measurement can be performed over a wide temperature and magnetic field range, at frequencies of 433, 866 and 1300 MHz. The system at Helmholtz-Zentrum Berlin (HZB) is based on a resonator built at CERN and has been optimized to lower peak electric fields and an improved resolution.

In this paper the design of an alternative calorimetry chamber is presented, providing flat samples for coating which are easy changeable. All parts are connected by screwing connections and no electron beam welding is required. Furthermore this design enables exchangeability of samples between the resonators at HZB and CERN.

First measurements with the new design show ambiguous results, partly explainable by RF losses at the indium gasket.

INTRODUCTION

In order to measure the RF surface resistance of circular planar samples the Quadrupole Resonator (QPR) was invented at CERN [1, 2]. In 2014 a second resonator was commissioned at HZB which is improved mainly towards a higher magnetic field on the sample surface and a lower peak electric field [3].

The QPR consists of a pillbox-like screening cavity with four vertical rods inside which are connected pairwise by crescent-shaped pole shoes (see Fig. 1). These pole shoes are placed at small distance (0.5 mm) above the sample surface and provide focusing of the RF magnetic field to that area. The length of the rods is adjusted to λ/2 of the baseline operation frequency of 433 MHz. Higher harmonics at 866 MHz and 1.3 GHz can be excited as well. For operation the resonator is cooled down to liquid helium temperature using a helium bath cryostat. The quadrupole rods are hollow, allowing liquid helium to cool these regions of high magnetic field.

The cylindrical calorimetry chamber is inserted into the resonator from below. The outside planar face of the calorimetry chamber facing the bottom of the rods is the sample. The calorimetry chamber itself acts as inner conductor of a coaxial structure which provides thermal decoupling of sample and resonator. Local heating of the sample using a DC heater attached to its bottom is used to set/change the temperature of it without changing the properties of the remaining resonator. All operation frequencies of the QPR are below the cut-off of the coaxial structure, hence significant RF heating of the calorimetry chamber is only located on the sample surface.

*sebastian.keckert@helmholtz-berlin.de

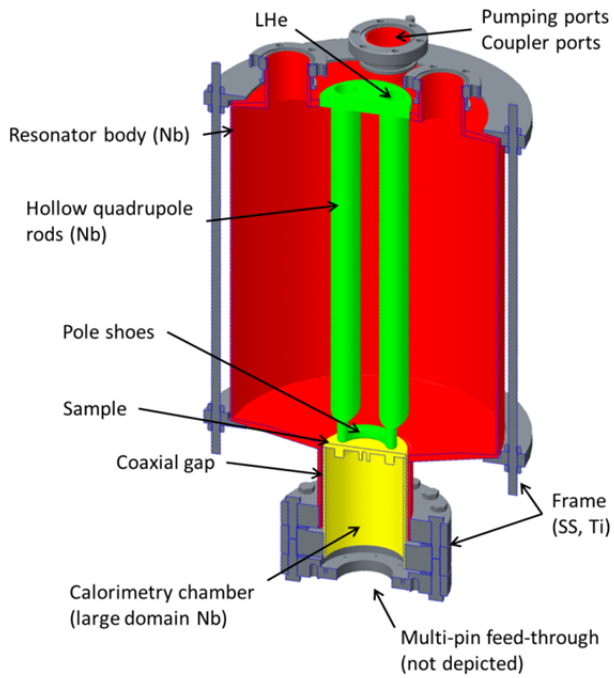

Figure 1: Schematic view of the Quadrupole Resonator in the plane of mirror. Each pole shoe connects two quadrupole rods (green colored) and focuses the RF magnetic field onto the sample surface (yellow) [4].

This enables the calorimetric measurement of the RF surface resistance. A direct RF measurement is less precise due to the strong coupling of the input coupler. Using the DC heater the sample is heated up to the temperature of interest and the heater power is measured. For temperature measurement calibrated Cernox™ sensors are attached to the sample at the regions of high magnetic field. In thermal equilibrium the RF is switched on and the heater power is reduced such, that the temperature of the sample again reaches the initial value. In steady state the heater power is measured again and the RF dissipation is given by the difference of DC heater power. Using a weakly coupled field probe the magnetic field strength is measured and the surface resistance is calculated according to

$$R_S = \frac{2\mu_0^2(P_{\mathrm{DC1}} - P_{\mathrm{DC2}})}{\int_{\mathrm{Sample}} |B|^2 dS} = \frac{2c\omega\mu_0^2(P_{\mathrm{DC1}} - P_{\mathrm{DC2}})}{Q_t\, P_t}$$

ISBN 978-3-95450-178-6

with the constant c known from simulations and the field probe quality factor Q_t. The transmitted power P_t is measured using the field probe. A sub-nΩ measurement resolution has been demonstrated [5, 6].

DESIGN OF THE ALTERNATIVE CALORIMETRY CHAMBER

In the existing design of the calorimetry chamber the niobium parts are electron beam welded and brazed into the bottom flange. In the new design, a thin sample holder ready for coating with superconducting thin films is available (see Fig. 2). Niobium tube and bottom flange are also made demountable in order to gain flexibility on the mounting height. By preparing different flanges the distance between sample surface and quadrupole pole shoes can be adjusted within few 100 µm which has significant impact on the RF field strength on the sample surface [3, 4]. Furthermore, this design enables exchangeability of samples between the resonators at HZB and CERN. The mounting height of these resonators differs by 3.5 mm which can easily be compensated using individually adapted bottom flanges.

In the design process of the demountable calorimetry chamber, numerical simulations were used to estimate the influence of imperfections at the contact area of the niobium parts on the RF fields. These simulations and consequential design considerations are discussed in the following.

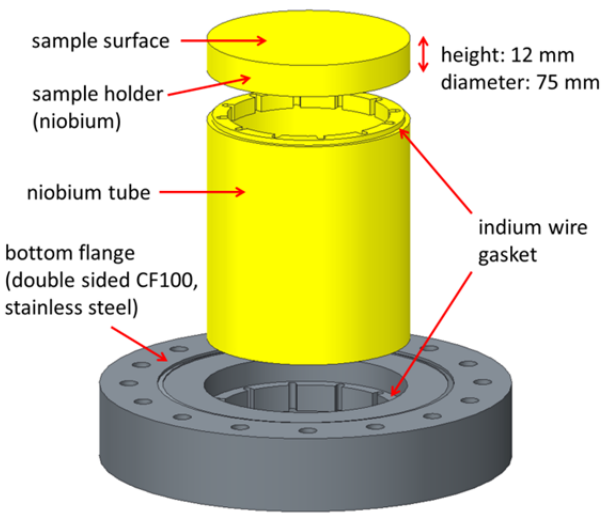

Figure 2: Exploded view of the alternative calorimetry chamber. The sample holder is a disk of 12 mm height and 75 mm diameter with the sample surface on top and threads for assembly and sensor mounting on its bottom. Indium wire gaskets are used in order to achieve RF and vacuum tight connections of all parts [4].

RF Simulations

In the design of a demountable calorimetry chamber one has to assume that the outer surface of the chamber cannot remain perfectly smooth. Since the local RF field is very sensitive to surface effects, possible issues have to be considered in the design process. Looking at the outer surface of the chamber, a separability results in two touching cylinders with "something" in between. That "something" at the contact area of the cylinders can contain any imperfection, potentially causing RF issues while measuring with the QPR. In the simulations discussed below only the contact area of sample holder and niobium tube are investigated. By construction the RF fields at the bottom flange are negligible, hence a contact area there will not cause any disturbing RF effect.

One important question to be answered by these simulations is what the minimum height of the sample holder must be. For coating, the minimal height is desired but then the contact area of the chamber parts is moved into a region of higher RF field. Crucial design criterion is to ensure safe operation of the QPR up to high fields, meaning that any additional power dissipation with impact on the temperature distribution of the sample has to be avoided.

This study was performed using a 3-dimensional model of the QPR and the computer program COMSOL Multiphysics (v. 4.4), which is a finite element solver.

A worst-case scenario is given by a circumferential gap between upper and lower part of the calorimetry chamber. Figure 3 shows the magnetic field strength on the (outer) surface of the calorimetry chamber as a color plot with the surface currents depicted by red arrows. On the sample the field is focused by the quadrupole pole shoes and the current flows circularly. On the walls of the calorimetry chamber the magnetic field strength decays exponentially with increasing distance into the coaxial structure, since the operation frequency is below cutoff. The maximum field in the coaxial structure is, in contrast to the sample, located at the opening between the pole shoes. At minimum and maximum magnetic field the surface currents flow parallel to the gap, leading to a quick decay of magnetic field inside the gap. At these positions, RF losses on an indium gasket which is placed at a distance d > 1 mm to the opening of the gap may be neglected.

At four locations however, the surface currents flow perpendicular to the gap. This leads to constant magnetic field inside the gap, independent of height and/or depth of the gap (see Fig. 3). In order to suppress RF losses on the indium gasket a circumferential gap is to be avoided.

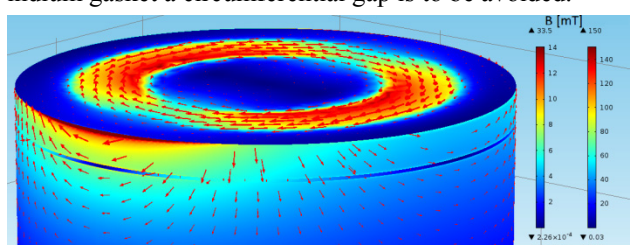

Figure 3: Color plot: Magnetic field on the surface of the calorimetry chamber. Surface currents are shown as red arrows. The solution is normalized to 150 mT peak field on the sample surface. Note: Length and color scales are different for sample (right color scale) and chamber surface (left scale) [4].

In order to estimate the maximum acceptable size of imperfections at the position of surface currents flowing perpendicular to the gap, further simulations with limited gaps of different width were performed. For gap widths smaller than 2.5 mm a damping of RF magnetic field above 90 % is achieved (see Fig. 4). Height and depth of the gaps have no significant influence on that.

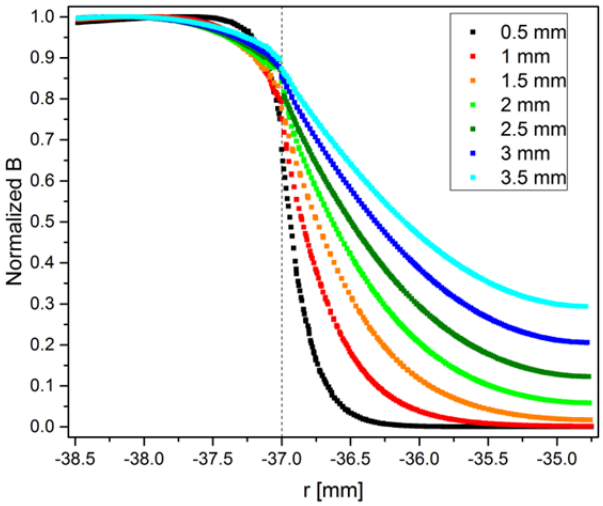

Figure 4: Normalized magnetic field in a limited gap of 2.25 mm depth and 0.5 mm height for different values of gap width. The magnetic field is plotted on a cut line in radial direction, entering the gap from left to right. The entrance of the gap is highlighted by a dashed line. The upper edge of the gap is located 5 mm below the sample surface [4].

In addition to the magnetic field penetrating imperfections at the contact area of the chamber parts, magnetic field enhancement (MFE) at these locations is considered. Scenarios of limited or circumferential gaps can be compared to bumps or well-like pits investigated at SRF cavities [7, 8]. A minimal rounding radius of these structures is estimated at 1 µm, according to [9]. If the ratio d/h of depth d and width w of a gap is larger than 0.75 the limit of "deep" holes may be applied. In this case the MFE factor β is given by [8]

$$\beta(h_{\mathrm{gap}}) = 0.47\,(h_{\mathrm{gap}}[\mu\mathrm{m}])^{1/3}.$$

This magnetic field enhancement is confined spatially within 0.5 mm.

In order to determine the height of the sample holder, it was decided to retain all dimensions unchanged which are relevant for measurements, i.e. placement of central heater and temperature sensors. This defines the minimal height of the sample holder to be 12 mm. In case of a peak magnetic field of 150 mT on the sample surface as presented above, the magnetic field strength in the coaxial structure at that position amounts to 2.80 – 4.35 mT. For gaps smaller than 250 µm the resulting MFE factor is smaller than 3, yielding a surface peak field of less than 15 mT confined to a sub-mm small region around a sharp edge. A field strength more than one order of magnitude lower than on the sample surface on an area of negligible size was accepted.

Bolting and Indium Gasket

Sample holder and niobium tube are connected via inlying bolting. Due to the malleability of niobium, helical screw thread inserts made of CuSn6 are used instead of niobium threads. The thread inserts inside of the sample holder are placed in a ring, separated from the one where the temperature sensors are mounted. This ensures that heat, generated by both DC heater and RF dissipation, is transported on a path similar to the existing sample design. In this way temperature profiles of the different sample holder designs differ as little as possible.

Following the design of the existing calorimetry chamber the tube wall thickness of 2 mm remained unchanged. At the top level of the tube a positive offset of 2 mm is implemented which provides easy positioning and centering of the sample. The mating part to the bolting of the sample holder is done using open slotted holes in order to vent the threads.

The indium wire gasket at the joint of sample holder and niobium tube is hidden in a void of triangular cross-section which is implemented by removing a small chamfer of the mating part at the sample holder (see. Fig. 5). The resulting hollow space is dimensioned to include 90 % of a wire which is 0.5 mm in diameter. The remaining 10 % are intended to compensate for possible flatness imperfections without causing any disturbing gap between sample holder and niobium tube.

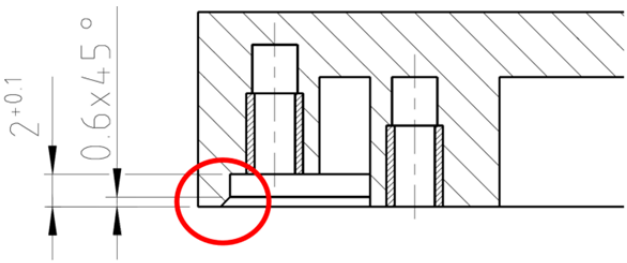

Figure 5: Implementation of the upper Indium gasket. The chamfer is highlighted by a red circle [4].

At the bottom level of the niobium tube, the wall thickness is increased to include threads for bolting the tube to the bottom flange. Instead of helical screw thread inserts tapped bushings made of titanium grade 2 are used and laser welded into the niobium tube. These bushings are positioned close to the outer edge of the tube to maximize the internal diameter. This is important to provide access to the bottom of the sample for sensor mounting after assembly of the chamber. The tapped bushings are open at the top end to ensure proper evacuation. As bottom flange a CF DN100 blank flange is used and adapted. An indium wire of 1.0 mm diameter is used to achieve a vacuum leak tight connection. Since RF effects are negligible at this location, the indium wire is simply pressed between niobium tube and flange. The offset in mounting height of the assembled chamber due to this gasket can be determined by measuring the shift of resonant frequency

ISBN 978-3-95450-178-6

of the QPR. By adapting the flange the distance between sample surface and quadrupole pole shoes can be adjusted within few 100 µm.

For both joints bolts made of titanium grade 5 are used. Titanium is especially suitable since its integral thermal contraction for a cool-down from room temperature to about 2 K is nearly the same as the one of niobium.

Production and Surface Treatment

The niobium parts were manufactured from large grain ingot niobium, RRR 300. Both parts were cut from a solid cylinder. It is known that after manufacture the surface layers of niobium are damaged and contaminated, which has big impact on the RF properties. In order to restore an intact surface and to further remove impurities a buffered chemical polishing (BCP) was performed after ultrasonic cleaning [10], removing 150 µm of material. The RF properties of the niobium tube are less important, hence only 40 µm were etched.

After BCP, the calorimetry chamber was assembled and leak tested. The required maximum leak rate of 10^{-7}mbar l/s could not be achieved without a gap between sample holder and niobium tube at the upper indium gasket. Due to material removal by BCP the cross-section of the chamfer to be filled by indium was increased. In order to restore the required leak rate, indium wire of 1 mm diameter was used leading to gap between sample holder and niobium tube.

After successful leak tests of the calorimetry chamber at room temperature and under liquid nitrogen, a 5 bar rinse using ultrapure water and ethanol constituted the last step of surface treatments before mounting into the QPR.

RF MEASUREMENTS

First RF measurements were performed using the QPR at CERN. The resonant frequency of the quadrupole resonator is sensitive to the distance between sample surface and quadrupole pole shoes. Comparing the measured value to RF simulations of the resonator yields a vertical offset due to both indium gaskets of 490 µm [4].

Surface Resistance

The RF surface resistance R_S of the new calorimetry chamber was measured twice, once at constant sample temperature with varying magnetic field (see Fig. 6) and vice versa (see Fig. 7).

The large values of R_S and the strong dependence on magnetic field strength are fully unexpected for a sample made of niobium RRR 300. At 4.0 K the surface resistance expected from BCS theory for the operation frequency of 400 MHz amounts to 43 nΩ [10]. The maximum magnetic field at which the surface resistance of the sample was measured was determined by RF heating of the sample. This is given, when the temperature of interest is achieved with RF dissipation only ($P_{DC2} \rightarrow 0$, i.e. the heater is switched off). The minimum field is given by RF measurement boundary conditions. The PLL system needs a non-zero field level for feed-back. Furthermore the RF measurement resolution at low field is limited due to the coupling of the field probe.

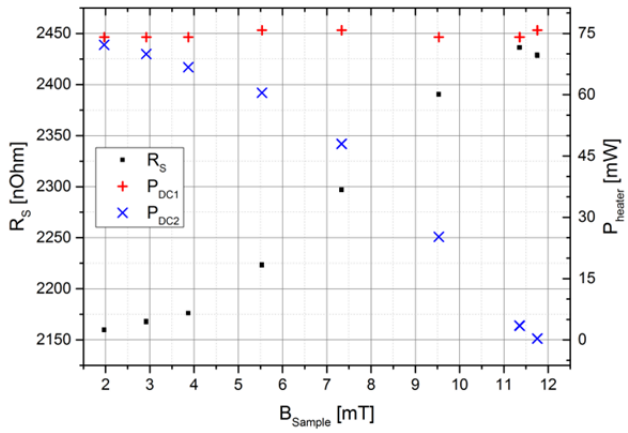

Figure 6: Surface resistance measurement at constant sample temperature T_{Sample} = 4.0 K. P_{DC1} denotes the DC heater power without RF dissipation, P_{DC2} the one in case of RF switched on and steady state reached again. The dissipated RF power is given by the difference. [4].

Measuring at constant RF field the minimum temperature of interest achievable is limited by RF heating of the sample. The results obtained at 5 mT show several unexpected aspects. Between 2.6 K and 3.0 K, the surface resistance is constant around 3170 nΩ. In the interval from 3.0 K to 3.3 K the resistance increases by 300 nΩ. Within 100 mK a steep decrease by 40 % is observed. From 3.5 K to 4.5 K the surface resistance increases by 60 nΩ.

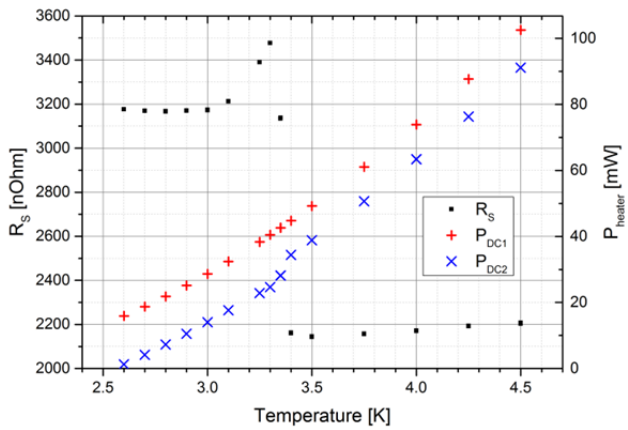

Figure 7: Surface resistance measurement at constant RF field B_{Sample} = 5 mT [4].

The discontinuity at 3.4 K is at the same temperature as the critical temperature of indium. The higher resistance below 3.3 K can be explained qualitatively by direct RF losses in the circumferential gap at the upper vacuum seal. Approaching T_c, the critical field goes to zero, leading to a quench of indium even at low magnetic field. The abrupt decrease of surface resistance above 3.4 K is caused by reduction of RF dissipation as clearly visible from P_{DC2}. This cannot be explained by the surface resistance of indium. Above 3.4 K normal conducting indi-

um would lead to a contribution of RF dissipation, approximately independent on temperature. A possible impact of thermal properties of indium can be excluded, since no phase transition is observed in DC heater power with RF switched off (P_{DC1}). Between 3.5 K and 4.5 K the surface resistance increases by 60 nΩ. The BCS expectation for niobium at 400 MHz in this temperature range amounts to 35 nΩ [10], which is close to the measured value.

Penetration Depth and RRR

The RF penetration depth is determined employing the shift of resonant frequency while heating the sample. This shift is measured using a vector network analyzer. Above 7.5 K a significant shift is observed and a fit is performed in the interval between 7.75 K and 9.1 K. The fit yields $\lambda_0 = (32.5 \pm 0.7)$ nm. From λ_0 electron mean free path and RRR are derived. A value of RRR $= 720_{-420}$ is obtained. Since the value of λ_0 is compatible with the London penetration depth $\lambda_L = 32$ nm within its uncertainty only a lower boundary can be given for RRR.

A measurement of the RF surface resistance in the normal conducting state at 13 K is compatible with the limit of anomalous skin effect which also indicates a RRR larger than 300.

Stylus Profilometry Measurement

The optical impression of the sample surface after BCP was unexpected, if compared to SRF cavities made of large grain niobium. In order to study the surface structure, a profilometry characterization of different areas was performed using a stylus profiler. A stylus with radium 2 µm was used, applying a force of 5 mg to the sample surface.

The sample surface is mainly occupied by large areas of matt or shiny surface, which are in the order of cm^2. Typical structures of the surface profile are obtained from scans at these locations, where periodic structures with similar height of 2-3 µm peak-to-peak were found. These profiles are probably imprints of the turning, still visible after 150µm BCP. Further scans were performed at scratch-like structures in order to estimate the maximum height of structures present on the sample surface. The maximum height detected amounts to 11 µm.

Although SRF cavities used for accelerator applications are produced in a very different way [10], the surface roughness of cavities treated with BCP amounts to 5-10 µm peak-to-peak, which is similar to the one obtained here. A study on cavity cut-outs excluded the primary contribution of surface roughness to RF dissipation [11]. For this reason surface roughness on the sample surface is not expected to explain the high level of RF surface resistance observed.

CONCLUSION

An alternative calorimetry chamber for the HZB QPR was developed, providing samples of 12 mm height which are easy changeable. The parts are connected by screwing connections and sealed using indium wire gaskets. Flexibility in mounting height and exchangeability of samples between the resonators at HZB and CERN are achieved by adapting individual bottom flanges.

First RF measurements with the new design show unexpected high surface resistance and a strong dependence of R_S on magnetic field strength and on temperature. The results are partly explainable by RF losses at the indium gasket. A stylus profilometry measurement did not reveal any suspicious properties of the surface profile.

ACKNOWLEDGMENT

This work is part of EuCARD-2, partly funded by the European Commission, GA 312453.

REFERENCES

[1] E. Mahner et al., Rev. Sci. Instrum. **74**, 3390 (2003).
[2] E. Haebel et al., "The Quadrupole Resonator, Construction, RF System, Field Calculations and First Applications", in Proc. EPAC 1998, Stockholm, Sweden.
[3] R. Kleindienst, O. Kugeler, J. Knobloch, "Development of an Optimized Quadrupole Resonator at HZB", in Proc. IPAC 2013, Paris, France.
[4] S. Keckert, "Optimizing a Calorimetry Chamber for the RF Characterization of Superconductors", master thesis, University of Siegen, Germany, July 2015.
[5] R. Kleindienst et al., "Commissioning Results of the HZB Quadrupole Resonator", TUPB066, SRF 2015, Whistler, Canada.
[6] S. Aull et al., "High Resolution Surface Resistance Studies", in Proc. SRF 2013, Paris, France.
[7] V. Shemelin, H. Padamsee, "Magnetic Field Enhancements at Pits and Bumps on the Surface of Superconducting Cavities", TTC-Report 2008-07, SRF 080903-04, 2008.
[8] T. Kubo, "Models of the Magnetic Field Enhancement at Pits", arXiv:1308.3311, 2013.
[9] J. Knobloch et al., "High-Field Q-Slope in Superconducting Cavities Due to Magnetic Field Enhancement at Grain Boundaries", in Proc. SRF 1999, Santa Fe, USA.
[10] H. Padamsee, J. Knobloch, T. Hays, *RF Superconductivity for Accelerators*, 2nd edition, Wiley, 2008.
[11] O. S. Romanenko, "Surface Characterization of Nb Cavity Sections – Understanding the High Field Q-Slope", PhD thesis, Cornell University, USA, 2009.

ISBN 978-3-95450-178-6